Explicit modelling of isoprene chemical processing in polluted air masses in suburban areas of the Yangtze River Delta region: radical cycling and formation of ozone and formaldehyde

Kun Zhang [a, b], Ling Huang [a, b], Qing Li [a, b], Juntao Huo [c], Yusen Duan [c], Yuhang Wang [d], Elly Yaluk [a, b], Yangjun Wang [a, b], Qingyan Fu [c], Li Li [a, b*]

[a] School of Environmental and Chemical Engineering, Shanghai University, Shanghai, 200444, China

[b] Key Laboratory of Organic Compound Pollution Control Engineering, Shanghai University, Shanghai, 200444, China

[c] Shanghai Environmental Monitoring Center, Shanghai, 200235, China

[d] School of Earth and Atmospheric Sciences, Georgia Institute of Technology, Atlanta, GA, USA

Correspondence to Li Li (Lily@shu.edu.cn)

Abstract

In recent years, ozone pollution has become among the most severe environmental problems in China. Evidence from observations have showed increased frequency of high O_3 levels in suburban areas of the Yangtze River Delta (YRD) region. To better understand the formation mechanism of local O_3 pollution and investigate the potential role of isoprene chemistry in the budgets of RO*x* ($OH+HO_2+RO_2$) radicals, synchronous observations of volatile organic compounds (VOCs), formaldehyde (HCHO) and meteorological parameters were conducted at a suburban site of the YRD region in 2018. Five episodes with elevated O_3 concentrations under stagnant meteorological conditions were identified; an observation-based model (OBM) with the Master Chemical Mechanism was applied to analyze the photochemical processes during these high O_3 episodes. The high levels of O_3, nitrogen oxides (NO*x*), and VOCs facilitated strong production and recycling of RO*x* radicals with the photolysis of

oxygenated VOCs (OVOCs) being the primary source. Our results suggest that, local biogenic isoprene is important in suburban photochemical processes. Removing isoprene could drastically slow down the efficiency of RO*x* recycling and reduce the concentrations of RO*x*. Besides, the absence of isoprene chemistry could further lead to decrease in the daily average concentration of O_3 and HCHO by 34% and 36%, respectively. Therefore, this study emphasizes the importance of isoprene chemistry in suburban atmosphere, particularly with the participation of anthropogenic NO*x*. Moreover, our results provide insights into the radical chemistry that essentially drives the formation of secondary pollutants (e.g. O_3 and HCHO) in the suburban of YRD region.

Keywords: Isoprene; Observation-based model (OBM); Radical; Ozone; Yangtze River Delta

1. Introduction

The hydroxyl radical (OH), hydro peroxy radical (HO_2) and organic peroxy radical (RO_2), collectively known as RO*x* dominate the oxidative capacity of the atmosphere and hence govern the removal of primary contaminants (e.g. volatile organic compounds (VOCs)) and the formation of secondary pollutants (e.g. ozone (O_3) , secondary organic aerosols (SOAs)) (Liu et al., 2012; Xue et al., 2016). RO*x* radicals can undergo efficient recycling (e.g. OH→ RO_2→RO→HO_2→OH) and produce O_3 and oxygenated VOCs (OVOCs) (Liu et al., 2012; Tan et al., 2019; Xue et al., 2016). In addition, the photolysis of OVOCs can in turn produce primary RO_2 and HO_2 radicals, and further accelerate the recycling of RO*x* (Liu et al., 2012). The reaction rates of different VOCs with RO*x* vary significantly (Atkinson and Arey, 2003; Atkinson et al., 2006). For instance, the reaction rate constants for OH with ethane and ethene are 0.248×10^{-12} (cm molecule^{-1} s^{-1}) and 8.52×10^{-12} (cm molecule^{-1} s^{-1}), respectively. Among the hundreds and thousands of VOC species, isoprene (C_5H_8, 2-methyl-1,3-butadiene) is among the most active and abundant biogenic VOCs (BVOCs) species globally (Wennberg et

al., 2018). Over the past decades, isoprene emission sources have been extensively studied (Gong et al., 2018) and recent works have focused on the degradation pathways and the impact of isoprene chemistry on regional forest chemistry (Gong et al., 2018; Wolfe et al., 2016a). Previous studies showed that isoprene could be quickly oxidized by atmospheric oxidants (e.g. OH, O_3 or NO_3) (Wolfe et al., 2016a; Gong et al., 2018; Jenkin et al., 2015). Due to the rapid reaction between OH and isoprene (100×10^{-12} cm^3 $molecule^{-1}$ s^{-1} at 298 K), more than 90% of the total daytime isoprene is removed via this reaction (Wennberg et al., 2018). The reaction between OH and isoprene is initiated by the addition of OH and can generate isoprene hydroxyperoxy radicals ($ISOPO_2$) (Wennberg et al., 2018; D'Ambro et al., 2017; Liu et al., 2013; Jenkin et al., 2015). $ISOPO_2$ isomers could then interconvert rapidly due to reversible O_2 addition and are finally removed via reactions with HO_2 or NO (Jenkin et al., 2015; Wolfe et al., 2016a). Hence, the degradation process of isoprene is tightly associated with RO*x* recycling. According to He et al. (2019), isoprene chemistry could strongly influence the photochemical formation of O_3, with a relative incremental reactivity (RIR) of ~0.06%/%. Besides, HCHO is also formed via several pathways during the depletion of isoprene (Jenkin et al., 2015; Wolfe et al., 2016a) and is found to be highly sensitive to isoprene emissions (Zeng et al., 2019).

The Yangtze River Delta (YRD) region is one of the most developed city-clusters in eastern China and is under serious O_3 pollution (Zhang et al., 2019; Zhang et al., 2020a; Chan et al., 2017). At the suburban area of YRD, high levels of O_3 have been frequently observed (Zhang et al., 2019; Zhang et al., 2020a). Several studies have investigated the relationship between O_3 and its precursors (Chan et al., 2017; Lin et al., 2020; Zhang et al., 2020a; Zhang et al., 2020b), but few studies have addressed the atmospheric oxidizing capacity and radical chemistry involved in these complicated photochemical processes (Tan et al., 2019; Zhu et al., 2020b). Previous studies have pointed out that the high levels of O_3 at suburban areas of

Shanghai could be attributed to the transport of O_3 or its precursors from urban areas (Lin et al., 2020; Zhang et al., 2019; Li et al., 2016; Li et al., 2019). On the contrary, high O_3 concentrations were frequently observed in suburban areas under stable meteorological conditions. Therefore, given the dense vegetation cover in suburban YRD and weak transport of air masses, the importance of local isoprene chemistry regarding ozone formation remains unclear.

In this study, we conducted a comprehensive set of in-situ observations of isoprene concentration, meteorological conditions, and concentrations of atmospheric pollutants (including O_3, NO_x, CO, VOCs, and HCHO) to understand the impact of isoprene chemistry on atmospheric photochemical processes in suburban YRD region. We used an observation-based model (OBM) to explore the role of local isoprene chemistry in radical budgets and the formation of O_3 and HCHO. Results from this study provides insights into the isoprene chemistry in the suburban region of a fast-developing city-cluster.

2. Methodology

2.1 Field measurement

The observations were conducted at a supersite (120.98°E, 31.09°N) in the suburban areas of the YRD region (Figure 1). It is located in the west of Shanghai and is close to the Dianshan Lake Scenic area, with relatively higher vegetation cover than the urban areas. To investigate the local isoprene chemistry and its influence on O_3 and HCHO formation, continuous measurements were conducted from April 7th to September 25th, 2018, when photochemical activity and O_3 formation is significant.

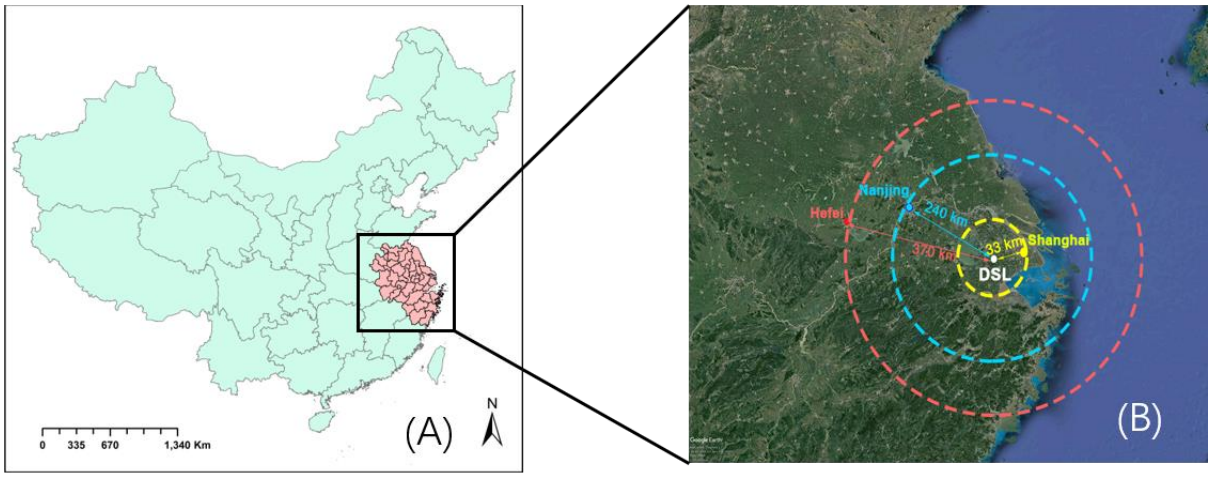

Figure 1. (A) map of China with YRD region highlighted in pink; and (B) satellite map of YRD region (created with Google Earth© on 23rd July 2020).

Table 1. Measurements performed during the ozone season.

Species/Parameter	Experimental Technique	Time resolution	Lower Detectable limit
O_3	Model 49i, Thermo Fischer Scientific, USA	60 s	0.5 ppbv
NO and NO_2	Model 42i, Thermo Fischer Scientific, USA	60 s	0.4 ppbv
CO	Model 48i, Thermo Fischer Scientific, USA	60 s	40 ppbv
HCHO	AL4021, Aero-Laser, GER	90 s	0.1 ppbv
VOCs species	GC866, Agilent., USA	1 hour	-
Temperature, relative humidity, wind speed and wind direction	Meteorological station, Vaisala, FIN	60 s	-

The measuring instruments are shown in Table 1. Wind speed (WS), wind direction (WD), ambient pressure (P), temperature (T), and relative humidity (RH) were simultaneously observed by a meteorological station (Vaisala., FIN). According to China's air quality standard, several criteria air pollutants were measured during this experiment. For instance, O_3 was measured by an ultraviolet photometric analyzer (Model 49i, Thermo Fischer Scientific., USA), with a detection limit of 0.5ppbv, whereas nitrogen oxides (NO and NO_2) were simultaneously observed by a chemiluminescence instrument (Model 42i, Thermo Fischer Scientific., USA), with a detection limit of 0.4ppbv. Likewise, carbon monoxide (CO) was monitored by a gas filter correlation infrared absorption analyzer (Model 48i, Thermo Fischer Scientific., USA), with a detection limit of 0.04ppm. All the online instruments used for gas analyzer were auto-

zero every day, and were multi-point calibrated every month. All the instruments used for the online observation were housed on top of a 5-floor-high building, which was about 15 m above the ground level.

A total of 55 VOC species, including 28 alkanes, 10 alkenes (including isoprene), 16 aromatics and acetylene were continuously analyzed at our sampling site by two online gas chromatographs with flame ionization detector (GC-FID) systems (GC-866 airmoVOC C_2-C_6 #58850712 and airmoVOC C_6-C_{12} #283607112, Agilent., USA) with a time resolution of 1 hour during the study period. Ambient samples are directly inhaled into this system by a pump. Low carbon VOCs (C_2-C_6) are captured by a low temperature (-10 °C) pre-concentration system, while high carbon VOCs are concentrated by a built-in room temperature pre-concentration system. Then the preconcentration system are heated and desorb VOCs, which are eventually carried into the chromatographic columns by helium. Individual VOCs separated in the columns are eventually detected by FID systems. Formaldehyde (HCHO) was continuously measured by a Hantzsch fluorescence technique (AL4201, Aerolaser GmbH., GER), which is based on fluorometric Hantzsch reaction in the liquid phase, requiring the quantitative transfer of HCHO from gas phase to liquid phase. A Hantzsch reagent (acetylacetone) was used in this instrument.

2.2 Observation-based model

In this study, a zero-dimensional (0-D) box model (F0AM) (Wolfe et al., 2016b) based on the University of Washington Chemical Model (UWCM) was used to simulate the atmospheric chemical processes. Dry deposition and atmospheric dilution were considered in this model. The Master Chemical Mechanism (MCM) v3.3.1 with more than 5,800 chemical species and 17,000 reactions was used in this study to enable a detailed description of the complex chemical reactions. In addition to gas-phase reactions, several heterogeneous processes including the uptake of HO_2, N_2O_5 and HCHO on aerosol surface as well as heterogeneous

sources of nitrous acid (HONO) were considered in our simulation. The rate constants and uptake coefficient of these reactions were obtained from the study of Riedel et al. (2014), Xue et al. (2014) and Li et al. (2014). Since key parameters such as aerosol surface area (S_A) and particle diameter (r) were not measured, an average S_A (640 nm^2/cm^3) was adopted from the field campaign in Shanghai (Wang et al., (2014)).

Table 2. Heterogenous reactions and associated rate constants used in the OBM model.

Reactions	Reaction rate constant	Reference
$N_2O_5 \rightarrow CLNO_2 + HNO3$	$\gamma\omega S_A/4$ (for $CLNO_2$ formation) $(2-\emptyset)\gamma\omega S_A/4$ (for HNO_3 formation)	Riedel et al. (2014)
$NO_2 \rightarrow HONO$	$k_g = \frac{1}{8} \times \omega\gamma_g(\frac{S}{V})$ $k_a = \frac{1}{4}\omega\gamma_a S_A$	Xue et al. (2014)
$HO_2 \rightarrow products$	$k = (\frac{r}{D_g} + \frac{4}{\gamma}\omega)^{-1} S_A$	Xue et al. (2014)
$HCHO \rightarrow products1$	$k = \frac{1}{4}\omega\gamma S_A$	Li et al. (2014)

γ= uptake coefficient for the given reactant with aerosol surface area; ϕ = product yield; ω=mean molecular speed of the given reactant (m/s); S_A=RH corrected aerosol surface area concentration (nm^2/cm^3); r=surface-weighted particle radius.

Photolysis frequencies (*J* values) were calculated by a trigonometric parameterization based on solar zenith angle (SZA):

$$J = Icos(SZA)^m \exp(-nsec(SZA)) \quad (1)$$

where *I*, *m* and *n* are constants unique to each photolysis reaction, derived from least-squares fits to *J* values computed with fixed solar spectra and literature cross-section and quantum yields (Wolfe et al., 2016b). Hourly average concentrations of speciated VOCs (except HCHO), NO, NO_2, CO and meteorological parameters (such as T, RH and P) were

151 used to constrain the F0AM model. Since nitrous acid (HONO) was not measured during our
152 observation, it was fixed as 2% of the observed NO_2 concentration. This constant ratio is well
153 observed in different field studies and performed well in previous box model studies (Tan et
154 al., 2019). Before each simulation, the model was run 3 days as spin up to reach a steady state
155 for unmeasured species (e.g., OH and NO_3 radicals).

156 The comparison of simulated and observed O_3 and HCHO concentrations are shown in
157 Figure S1 and Figure S2. The index of agreement (IOA), mean bias (MB) and normalized mean
158 bias (NMB) are used to evaluate the model performance. These three parameters can be
159 calculated by Equation (2) to (4), where S_i, O_i, and $\bar{O}$ are the simulated, observed, and average
160 observed value of the target compound. In this study, the IOA, MB and NMB of O_3 was 0.90,
161 0.76 and 10%, respectively. These results suggest that the model can reasonably reproduce the
162 variations of O_3 and could be used for further analysis. As for HCHO, the IOA, MB, and NMB
163 was 0.74, 2.43 and 48%, respectively. In general, the model overestimated HCHO
164 concentration, especially on July 29 and July 30. According to previous studies, the
165 inconsistency between simulated and observed HCHO is attributed to uncertainties in the
166 treatment of dry deposition, faster vertical transport, uptake of HCHO and fresh emissions of
167 VOCs precursors (Li et al., 2014). In addition, primary HCHO sources can contribute up to 76%
168 of total HCHO concentration in urban areas (Li et al., 2010). However, due to the lack of
169 primary HCHO sources for areas around DSL, primary HCHO emissions were not included in
170 our model. Although there exists some bias, the model results still provide valuable information
171 of secondary formation of HCHO at suburban areas. To assess the reliability of model results
172 without OH observation, we compared the OBM-simulated OH concentration with that
173 calculated using the ratio of ethylbenzene (E) and m,p-xylene (X) that share common emission
174 sources but with different reactivity with OH radicals (shown in Equation (5)~(8)):

$$IOA = 1 - \frac{\sum(S_i - O_i)^2}{\sum(|S_i - \bar{O}| + |O_i - \bar{O}|)^2} \quad (2)$$

$$MB = \frac{\sum(S_i - O_i)}{N} \quad (3)$$

$$NMB = \frac{\sum(S_i - O_i)}{\sum O_i} \times 100\% \quad (4)$$

$$Ethylbenzene + OH \rightarrow products \qquad k_{Ethylbenzene,OH} = 7.0 \times 10^{-12} \quad (5)$$

$$m,p - Xylene + OH \rightarrow products \qquad k_{m,p-Xylene,OH} = 1.89 \times 10^{-11} \quad (6)$$

$$[X]_t = [X]_0 \times e^{-[OH] \times k_{X,OH} \times t} \times f_{d,B} \quad (7)$$

$$[OH]_{\frac{E}{X}} = \frac{1}{t \times (k_{E,OH} - k_{X,OH})} \times [ln\left(\frac{[E]}{[X]}\right)_0 - ln(\frac{[E]}{[X]})_t] \quad (8)$$

where $[X]_0$ and $[X]_t$ are the mixing ratio of X at the initial time and after transport time t. $k_{X,OH}$ is the temperature dependent reaction rate coefficient of m,p-xylene with OH, which was taken from the IUPAC database (http://iupac.pole-ether.fr/), whereas $f_{d,B}$ is the dilution factor of m,p-xylene in the atmosphere. In this study, we assume that the rates of turbulent mixing and horizontal convection are similar for E and X. Therefore, during the transport time Δt, the dilution factor of E and X are the same. Therefore, rearranging Equation (7) and extending this analysis to E and X will yield Equation (8), where $[OH]_{E/X}$ is the estimated regional mixing ratio of OH by ethylbenzene and m, p-xylene ratio. The calculated average regional concentrations of OH (8.39 ± 5.11 ×10^6 molecules cm^{-3}) was in the same magnitude of the OBM-simulated result (4.59 ± 5.11 ×10^6 molecules cm^{-3}), suggesting that the OBM-simulated radical concentration is reliable.

To quantify the changes of atmospheric oxidative capacity (AOC) in response to isoprene chemistry, two parallel scenarios (S0 and S1) were conducted with isoprene chemistry disabled in S1. In both cases, identical chemical mechanism and meteorological conditions were used to drive the model simulations. A comparative analysis of the scenarios revealed the impact of isoprene chemistry on AOC and secondary formation of O_3 and HCHO.

3. Results and discussions

3.1 Overview of the observations

To investigate the impact of local chemistry on ozone formation and avoid the influence of emission transportation, five days under stagnant condition (with daily average wind speed less than 2m/s and maximum daily 8-h average (MDA8) O_3 concentration >75 ppb) were identified as typical local chemistry cases. Figure 2 shows the time series of observed meteorological parameters (P, T, and RH), trace gases (NO, NO_2 and O_3), isoprene and HCHO on selected days. During those episodes, the air masses reaching the site were mainly from southeast and southwest (Figure 2). The weak wind was not conductive to the regional transportation of air pollutants. The observed O_3, NO_2, NO, CO, and TVOC ranged from 1.40 to 155.40 ppbv (52.72 ± 44.43 ppbv, average value, the same below), 5.36 to 57.95 ppbv (21.58 ± 12.88 ppbv), 0.75 to 54.51 ppbv (5.40 ± 8.13 ppbv), 400 to 960 ppbv (597 ± 153 ppbv), and 2.34 to 20.33 ppbv (7.28 ± 4.32 ppbv) respectively. During the five episodes, the average concentration of alkanes (13.97 ± 9.12 ppbv), alkenes (3.27 ± 2.31 ppbv) and aromatics (4.93 ± 2.69 ppbv) was about 53%, 18%, and 50% respectively, higher than that of the whole observation period. The conditional probability function (CPF) is applied to reveal the relationship between high O_3 concentrations and wind (Figure 3). The detailed description of CPF can be found in the supplementary information (Text S1). The results suggest that high O_3 concentrations (>131 ppb) was usually observed when the site was influenced by weak south wind. This implies that the high O_3 was mostly formed locally. Although this site is distant from urban areas, high levels of NO were found during early morning, emanating particularly from nearby heavy-duty vehicle emissions. As for NO_2, only one peak was found at dusk. This was in contrast with previous results in urban areas (Zhang et al., 2019). It is worth noting that NO_2 and O_3 concentrations were high even during nighttime, suggesting that the AOC remained high at nighttime. It should also be noted that, flat CO pattern was found

during morning when NO*x* peaks were observed. This inconformity can be attributed to the coarse resolution of CO analyzer (about 80 ppbv) and CO emission source (mainly gasoline vehicles in terms of vehicle exhaust) while NO*x* is mainly emitted by heavy-duty vehicle exhausts. Therefore, since DSL site is far from urban area, it is unlikely to have gasoline vehicles in early morning. On the contrary, there are sometimes heavy-duty trucks passing by, causing peaks of NO in early morning.

The daily average isoprene concentration was 0.37 ± 0.36 ppbv, and is comparable to the observations by Gong et al. (2018) at a forested mountaintop site (0.287 ± 0.032 ppbv). To estimate the influence of isoprene on atmospheric oxidation capability, we adopted the approach by Zhu et al. (2020) to calculate the OH reactivity (k_{OH}). Results suggested that isoprene, accounting for ~19% of the total k_{OH}, was the most significant VOC species with respect to k_{OH} (0.89 ± 0.44 s-1). This indicates the significant role of isoprene in the photochemistry of a suburban area. The average HCHO was 5.01 ± 3.80 ppbv, which was ~2 times of that observed at a rural site of Hong Kong (Yang et al., 2020). It is worth noting that HCHO could reach an average of 18.69 ppbv at midday.

Based on explicit calculation, the total concentration of OVOC was obtained. However, due to the complexity of OVOC formation, which could have hundreds of precursors for just one OVOC specie and the complex chain reactions converting VOCs to OVOCs, it is difficult to derive an accurate relationship between VOCs and OVOCs. But since VOCs were mainly oxidized by OH and O_3 during daytime, in this study, we chose multi-linear regression model (Eq.(9)) to roughly explore the relationship between VOCs and simulated OVOCs.

$$[OVOC] = \beta_0 + \beta_1[Alkane] + \beta_2[Alkene] + \beta_3[Aromatic] + \beta_4[OH] + \beta_5[O_3] \quad (9)$$

where β_0, β_1, β_2, β_3, β_4, and β_5 are the coefficients from linear regression; [OVOC] and [OH] are the predicted concentration of OVOC and OH, respectively; [Alkane], [Alkene], [Aromatic], [O_3] are the observed concentration of alkanes, alkenes, aromatics, and O_3,

respectively. The Sig value and statistical reliability criteria (R) was 0.000 and 0.853 (shown in Table S2 and Figure S3), respectively, indicating that the linear relationship represented by equations (9) is statistically reliable. Similarly, the β_1, β_2, β_3 was 0.027, 0.623, and 0.820, respectively, suggesting that alkenes and aromatics are significant for the simulated OVOC concentration.

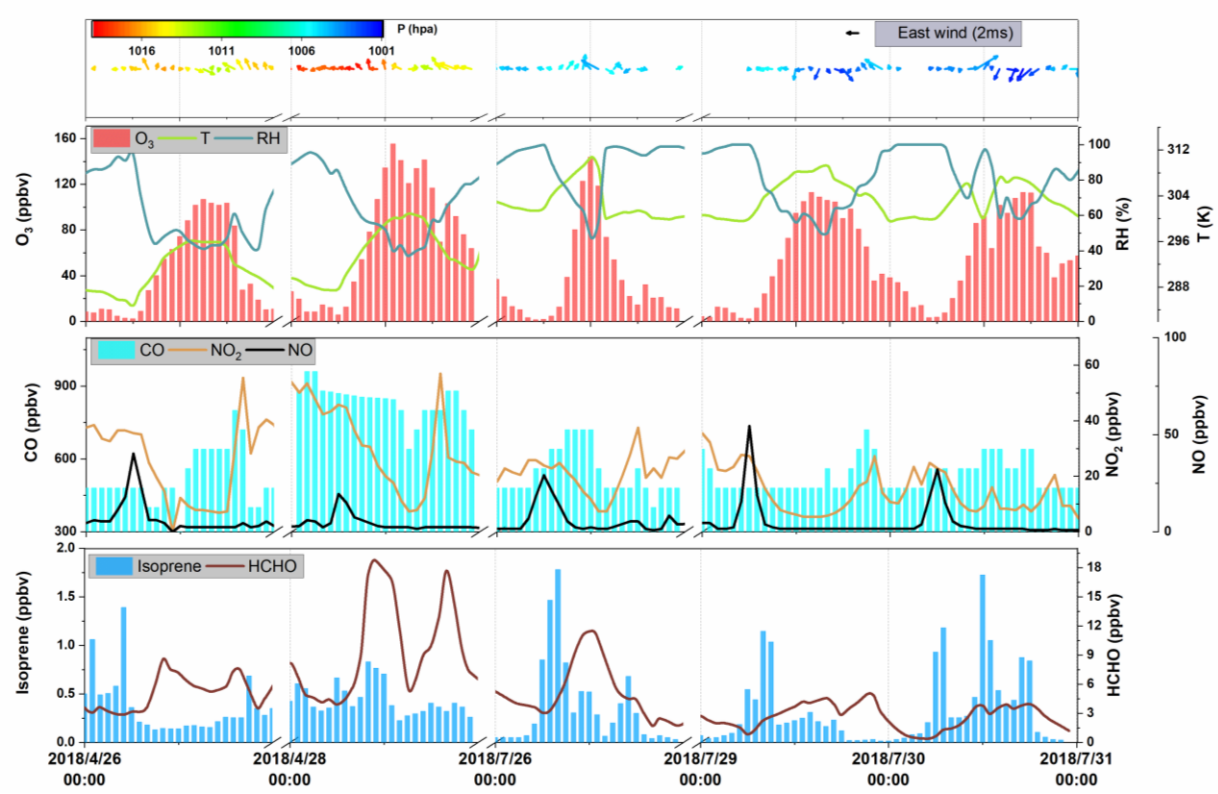

Figure 2. Time series of hourly averages for O_3, CO, NO, NO_2, isoprene, HCHO, and meteorological parameters.

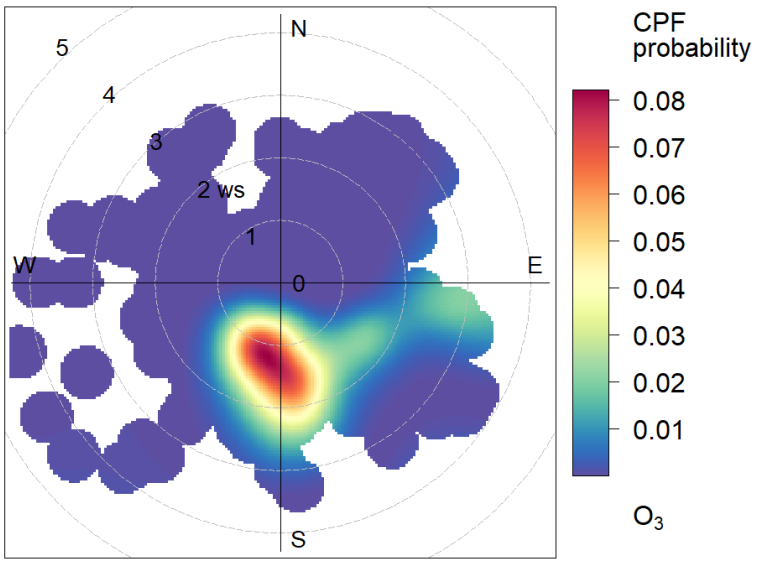

Figure 3. CPF polar plot of O_3 at DSL station.

3.2 Simulated concentrations of radicals

Figure 4 shows the simulated average daytime variation of major radicals in the base scenario (S0). It should be noted that, the discussion below is limited to local conditions (cases with average wind speed lower than 2m/s), since transportation of emissions are not considered in the 0-dimensional model. The daily average simulated concentration of OH, HO_2, RO_2, and NO_3 was 4.88×10^6, 3.49×10^8, 0.31×10^9, and 0.31×10^8 molecules cm^{-3}, respectively. The simulated daily average OH concentration is comparable to a summertime simulation in Beijing (9×10^6 molecules cm^{-3}) (Liu et al., 2019) and at a suburban site in Hong Kong in 2013 ($1.5 \pm 0.2 \times10^6$ molecules cm^{-3}) (Xue et al., 2016). In addition, the average simulated daytime OH concentration was ~33% lower than that simulated at a forested mountaintop site in southern China (Gong et al., 2018). To verify the performance of OBM model, regional daytime mixing ratios of OH were also calculated by a parameterization method using measured ethylbenzene and *m,p*-xylene ratios. The calculated average regional concentrations of OH ($8.39 \pm 5.11 \times10^6$ molecules cm^{-3}) was in the same magnitude of the OBM-simulated

result (4.88 ± 5.11 × 10^6 molecules cm^{-3}), suggesting that the OBM-simulated radical concentration is reliable. Furthermore, at the DSL site, the simulated maximum HO_2 concentration (6.19×10^8 molecules cm^{-3}) was close to that reported in Beijing (6.8×10^8 molecules cm^{-3}) (Liu et al., 2012), but was ~32% higher than that in Wuhan (4.7×10^8 molecules cm^{-3}) (Zhu et al., 2020a). Due to high reactivity of RO_2 and high concentration of HO_x, RO_2 kept low level during daytime. As for NO_3, it can be quickly decomposed during daytime, leading to the negligible concentration in the daytime.

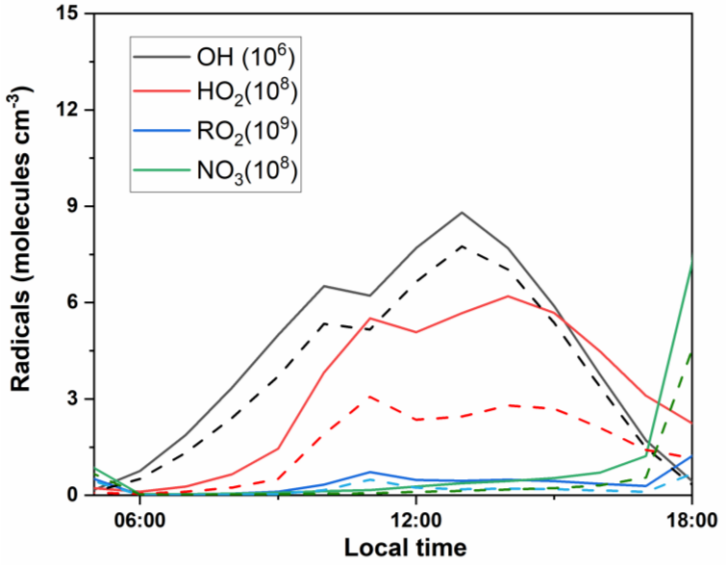

Figure 4. Simulated average daytime variation of OH, HO_2, RO_2 and NO_3 in S0 (solid lines) and S1 (dash lines).

3.3 Recycling of RO*x* radicals

Figure 5(A) shows the primary sources of RO*x* in S0 and its detailed daytime budget. Minor RO*x* sources, e.g. ozonolysis of alkenes, are not shown in the figure. Photolysis of O_3 was the predominant primary source of OH, with a daytime mean production rate of 0.50 ppbv h^{-1}, which was comparable to that found by Liu et al. (2012) in Beijing, but was 0.40 ppbv h^{-1} lower than the result reported by Xue et al. (2016). Similarly, another important OH source is the photolysis of HONO, contributing 0.32 ppbv h^{-1} of daytime OH production in our simulation. This result is much lower than other related studies (Liu et al. (2019) and Xue et al.

(2016)), possibly due to the excessive constrain on HONO (since HONO was not directly monitored) during our experiment.

Sensitivity analysis was conducted to quantify the influence of different $HONO/NO_2$ ratio on radical recycling (Text S2, Figure S4 and Table S1). As expected, a lower $HONO/NO_2$ ratio leads to a lower HONO concentration, and subsequently less OH generation from the photolysis of HONO. The sensitivity analysis shows that when $HONO/NO_2$ ratio is 0.005, the daytime OH level could decrease by 15.28%. Conversely, a higher $HONO/NO_2$ (e.g., 0.04) can promote OH concentration by 14.08%. This result illustrates the importance of HONO photolysis in the generation of OH, and therefore simultaneous ambient measurements of HONO is highly recommended for future analysis of local radical recycling. Regarding HO_2, the photolysis of OVOC (excluding HCHO) is the predominant source with a daytime mean production rate of 0.65 ppbv h^{-1} and maxima of 0.92 ppbv h^{-1}, which is comparable to Xue et al. (2016). The photolysis of HCHO can also contribute 0.48 ppbv h^{-1} to the daytime production of HO_2, which is close to the results of Xue et al. (2016). As for RO_2, the photolysis of OVOC was the largest source (0.57 ppbv h^{-1}), which was relatively lower than the results found at an urban site (Liu et al., 2012). Therefore, regarding RO*x* in DSL site, the daytime primary radical production was dominated by the photolysis of OVOC (except for HCHO), followed by the photolysis of HCHO and O_3. However, the photolysis of HONO can become the overwhelming RO*x* source around sunrise, which suggests that HONO can be an important OH reservoir species at night. Summing up all the sources of RO*x* gives a total primary daytime RO*x* production rate of 2.55 ppbv h^{-1} (0.84 ppbv h^{-1} for OH, 1.14 ppbv h^{-1} for HO_2, and 0.57 ppbv h^{-1} for RO_2), which was 61~69% lower than those in Beijing (6.6 ppbv h^{-1}, Liu et al. (2012)) and Hong Kong (8.11 ppbv h^{-1}, Xue et al. (2016)), indicating that the recycling of RO*x* in Beijing and Hong Kong could be much reactive.

306 RO*x* radicals are ultimately removed from the atmosphere via deposition of radical
307 reservoir species, e.g. H_2O_2, HNO_3, and ROOH (Liu et al., 2012). The terminate processes of
308 RO*x* was dominated by their reactions with NO*x*. Specifically in this study, the reaction of
309 OH+NO_2, RO_2+NO_2, RO_2+NO, forming HNO_3, RO_2NO_2, and $RONO_2$, accounted for 2.42,
310 0.56, and 0.41 ppbv h^{-1} of the daytime RO*x* radical sink, respectively. This is consistent with
311 the understanding that reactions with NO*x* usually dominate the radical sink under high NO*x*
312 environments (Xue et al., 2016; Liu et al., 2012). In addition, $RONO_2$ and RO_2NO_2 could in
313 turn react with OH, leading to 0.41 ppbv h^{-1} of daytime OH sinks (Figure 6). Summing up the
314 primary sources and sinks gives a negative value of net RO*x* production, suggesting that the
315 RO*x* was in a stage of gradual depletion.

316 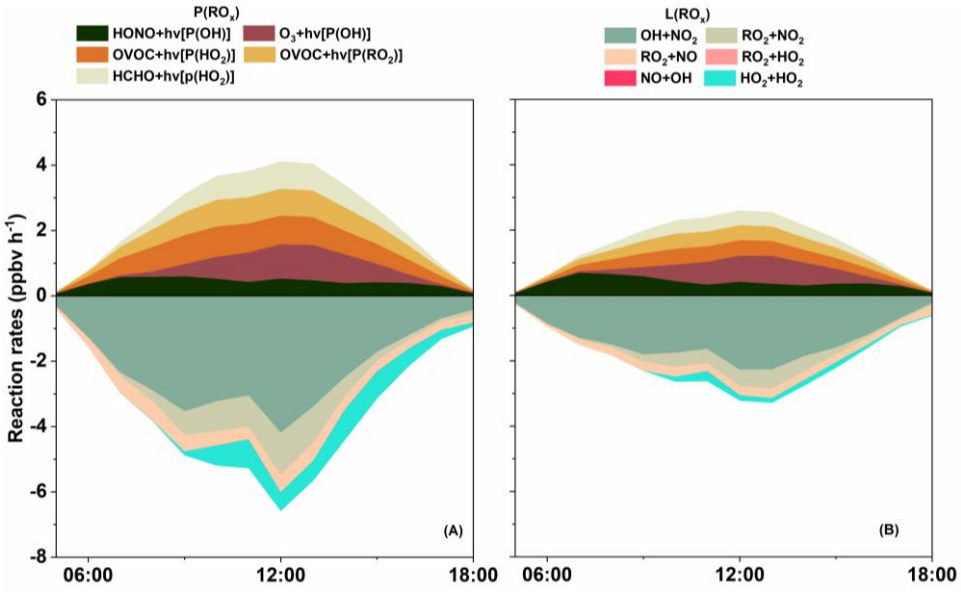

317 **Figure 5. Simulated primary daytime sources and sink of RO*x* in S0 (A) and S1 (B).**

318 Furthermore, the daytime (6:00-18:00) average budget of RO*x* is shown in Figure 6.
319 Evidently, the production of OH was dominated by the reaction of HO_2+NO (8.29 ppbv h^{-1})
320 in RO*x* recycling, whereas RO_2 was produced by the reaction of OH with OVOC (3.02 ppbv
321 h^{-1}), alkyl (RH) (1.21 ppbv h^{-1}), and peroxides (0.14 ppbv h^{-1}). Besides, the reaction of
322 RO_2+NO can result in strong production of RO (3.87 ppbv h^{-1}). Moreover, the reaction of RO
323 and O_2 was the major contributor to HO_2 production, followed by the reaction of OH with CO

(1.89 ppbv h^{-1}), OVOC (1.59 ppbv h^{-1}), and RH (0.15 ppbv h^{-1}). It is worth noting that the top two fast reactions within the recycling of RO*x* (HO_2+NO and RO_2+NO) were related to NO*x*. As mentioned in the study of Liu et al. (2012), this result could be mainly due to the abundance of NO (e.g. ~50 ppbv in the morning). Obviously, these recycling processes dominate the total production of OH, HO_2 and RO_2 radicals. As suggested in the study of Xue et al. (2016) and Liu et al. (2012), the radical propagation is efficient and enhances the effect of the newly produced radicals in the polluted atmospheres with the co-existence of abundant NO*x* and VOCs.

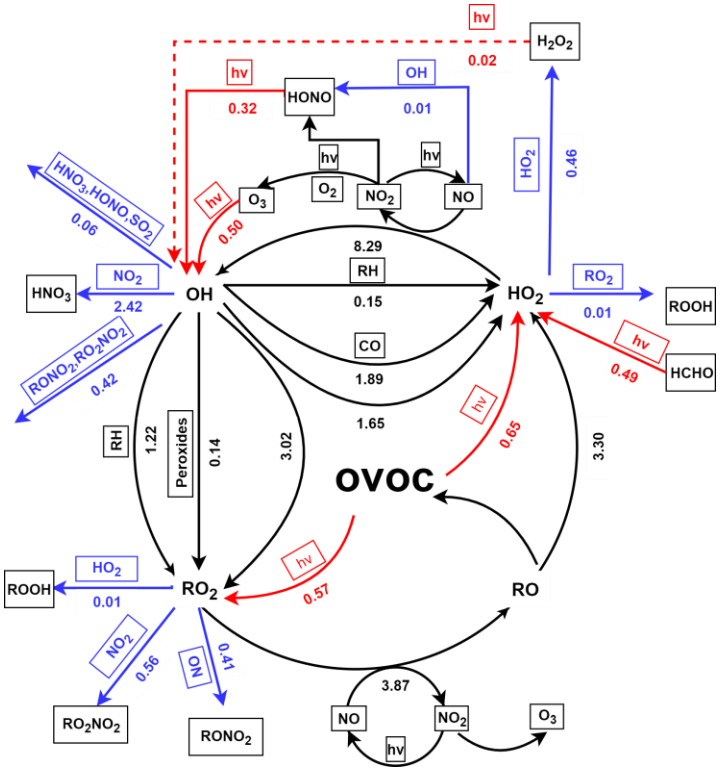

Figure 6. Summary of daytime (06:00-18:00) average budgets of RO*x* radicals (in ppbv h^{-1}). Primary RO*x* sources and sinks are in red and blue, respectively, and the black lines represent the processes in RO*x* and NO*x* recycling.

3.4 Formation and sink of O_3

Figure 7 illustrates the diurnal variation of simulated O_3 concentration, net production rate (including the formation and sink pathways) in S0. In the troposphere, O_3 is formed via the reactions of NO with peroxy radicals (e.g. HO_2 and RO_2) (Liu et al., 2012; Xue et al., 2016;

Zhu et al., 2020a). Consequently, the daytime reaction of HO_2+NO and RO_2+NO contributed an average of 9.34 and 8.52 ppbv h^{-1} of the O_3 produced. Coincidentally, the maximum rate of HO_2+NO (15.36 ppbv h^{-1}) and RO_2+NO (13.26 ppbv h^{-1}) both occurred at 13:00 LST. Our results reveal a total daytime production rate of O_3 ($P(O_3)$: the sum of HO_2+NO and RO_2+NO) at 17.86 ppbv h^{-1}, which is in line with related study in Beijing (32 ppbv h^{-1}, Liu et al. (2012)) and Hong Kong (6.7 ppbv h^{-1}, Liu et al. (2019)).

Due to the fast cycling of both O_3 and NO_2, the sink of O_3 resulted from several reactions leading to the destruction of O_3 and NO_2. In our case, the reaction of NO_2+OH is the predominant scavenging pathway of O_3, with an average daytime reaction rate of 1.89 ppbv h^{-1} (49%, percentage of the total O_3 sink rate.). This is comparable to the study of Liu et al. (2012 and 2019). In addition, the reaction of RO_2+NO_2 was the second contributor to O_3 sink with a mean contribution of 0.62 ppbv h^{-1} (16%). Other pathways, e.g. photolysis of O_3, ozonolysis of alkenes, and O_3+HO_2, altogether contributed 1.11 ppbv h^{-1} of the total daytime O_3 sink rate. Also, the daytime mean $L(O_3)$ was 3.87 ppbv h^{-1}, which was ~22% of $P(O_3)$, suggesting that O_3 could efficiently accumulate during daytime. The net production of O_3 ($P(O_3)$-$L(O_3)$) is also shown in Figure 7. Our results reveal a maximum O_3 concentration at around 16:00 LST, which was also observed in other suburban sites (Zong et al., 2018; Zhang et al., 2019).

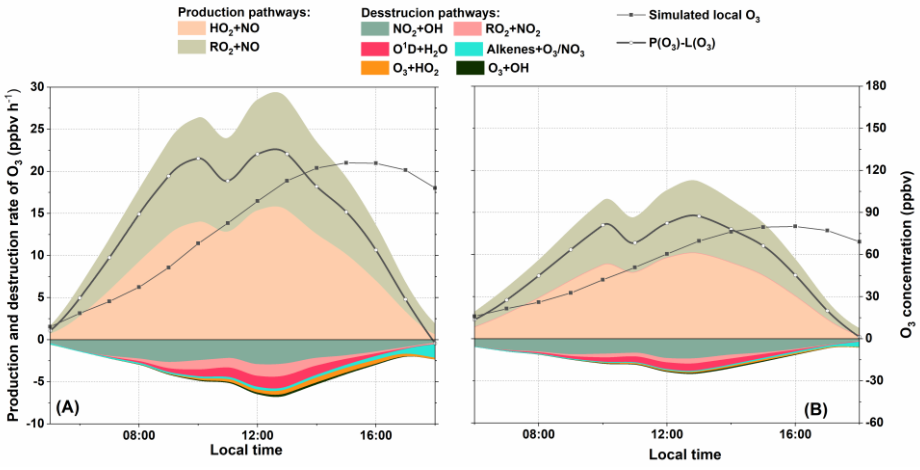

Figure 7. Simulated average diurnal profiles of O_3 formation and sink rates (ppbv h^{-1}) in S0 (A) and S1 (B).

3.5 Formation and sink of HCHO

As aforementioned, high levels of HCHO was observed at DSL. Figure 8 (A) shows the production and sink pathways of HCHO in S0. In this study, the local HCHO formation was dominated by the reaction of RO+O_2, accounting for ~90% of the total production rate. Further classification of RO+O_2 pathway suggested that the oxidation of CH_3O made a significant contribution of ~47%, followed by RO (from isoprene) + O_2 reaction (12%) and RO (from aromatics) + O_2 reaction (~11%). This result is comparable to the study of Yang et al. (2020; 2018). During the day, isoprene is the most important VOC species in the production of HCHO with a mean rate of 0.48 ppbv h^{-1}. As stated earlier, the study site is surrounded by dense vegetation, which provides abundant biogenic isoprene. As a result, over 90% of the daytime isoprene was oxidized by OH radicals (Figure S5). Based on the MCMv3.3.1, several RO_2 species (e.g. ISOP34O2, ISOPDO2, ISOPCO2, CISOPAO2, ISOPAO2) can be generated during the OH-initiated degradation process of isoprene (Jenkin et al., 2015). For instance, with the presence of NO, isoprene-originated RO_2 can transfer into RO (e.g. ISOPDO, ISOP34O, ISOPAO). The subsequent degradation processes of isoprene-related RO, especially ISOP34O, ISOPDO, ISOPAO and ISOPBO, are closely related to the formation of HCHO (Jenkin et al., 2015). In other sources of HCHO, such as the reaction between VOC and O_3, photolysis of OVOC and the reaction of OVOC+OH only contributed small amount of the total production rate during whole day.

In this study, it is noteworthy that the two dominant pathways for HCHO depletion were the photolysis of HCHO (~52%) and the reaction of HCHO+OH (~48%). On the other hand, the net HCHO production rate (equals to P(HCHO) + L(HCHO)) as shown in Figure 8. It is evident that after sunrise, the net production rate of HCHO rose gradually to a peak of ~1.6 ppbv h^{-1} at 8:00 (similar to the results by Yang et al. (2018)). Thereafter, at around 12:00 LST, net(HCHO) dropped to ~0 ppbv h^{-1}, which was roughly consistent with our observation,

showing the HCHO peak occurs at around 12:00. In addition, a negative net(HCHO) was exhibited between 13:00 and 14:00, . Although the reaction of $RO+O_2$ quickly produced HCHO in the afternoon, the depletion pathways, especially the photolysis of HCHO, became more competitive, leading to the net reduction of HCHO. This also indicates that strong photochemical reactions do not monotonously profit the accumulation of HCHO, it can also constrain high HCHO levels in certain situations. After 14:00, the photolysis of HCHO dropped rapidly and the net depletion of HCHO back to ~0 ppbv h^{-1} at around 15:00. The daytime net HCHO production rate was 0.70 ppbv h^{-1}, which was comparable to result of Yang et al. (2018).

The above analysis indicates that the photolysis of OVOC, HCHO, O_3 and HONO was the primary source of RO*x*, which offers high oxidizing environment for the degradation of VOCs. As a typical by-product in the degradation of several VOCs, HCHO can be quickly formatted during the day. The insight into the detailed photochemical processes shows the important role of isoprene in the formation of HCHO.

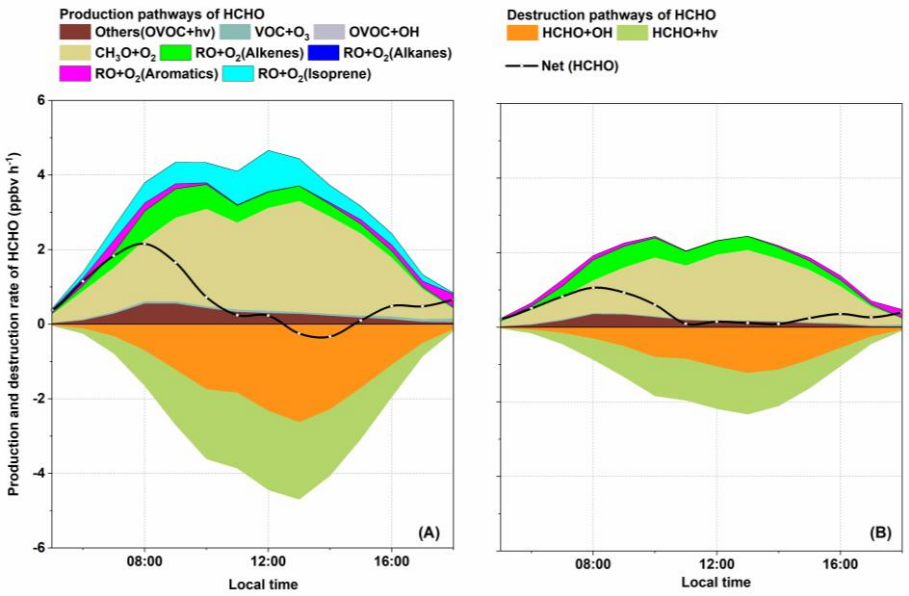

Figure 8. Simulated average daytime profiles of net rate (net (HCHO)), breakdown HCHO production rate and sink rate (ppbv h^{-1}) in S0 (A) and S1 (B).

3.6 Impacts of isoprene chemistry on photochemistry

3.6.1 Impact on RO*x* budget

To compare the importance of isoprene and other abundant VOCs in local chemistry at DSL site, sensitivity analysis was conducted for the modelled O_3, HCHO, and OH concentrations without the input of active VOCs (toluene, ethylene, ethylbenzene, ethane, acetylene, xylene, propene, and isoprene). Results suggested that, although the average isoprene concentration was only 0.37 ± 0.36 ppbv, cutting isoprene input can lead to obvious drop in simulated O_3, HCHO, and OH, which was comparable to that of cutting EXT and alkenes, indicating the significant role of isoprene in local photochemical processes (Figure S6). In addition, the degradation of isoprene is closely linked to the cycling of RO*x*. To roughly explain the impact of isoprene chemistry on RO*x* budget, we carried out a parallel simulation (S1) where isoprene chemistry is disabled (Figure 9). The diurnal variation of OH, HO_2, RO_2 and NO_3 in S1 is also shown in Figure 4 (B) which clearly suggests the decline in RO*x* and NO_3 without isoprene input. To investigate the underlying causes, we calculated the production rate of RO*x* (P(RO*x*)) and loss rate of RO*x* (L(RO*x*)) in S1, respectively (Figure 5 (B)). Comparative analysis revealed a decreasing trend for most of the reaction rates in P(RO*x*) and L(RO*x*) in S1. This strongly indicates that the absence of isoprene slows down the RO*x* recycling. Generally, considering that the photolysis of OVOC (0.67 ppbv h^{-1}) was still the predominant primary source of RO*x*, but without isoprene, the photolysis rate of OVOC decreased by 0.49 ppbv h^{-1}. Moreover, the total production and depletion rate of OH dropped to 6.96 and 7.51 ppbv h^{-1}, respectively. Although the absence of isoprene could reduce the consumption of OH, the OH concentration would be reduced by ~16% compared to S0, suggesting that the amount of OH produced via isoprene chemistry is large enough to compensate for the shift from OH to peroxy radicals in the RO*x* family. As for RO_2, the daytime production and sink rate falls to 3.25 and 3.34 ppbv h^{-1}, respectively. This means the

concentration of RO_2 would be in a stage of gradual decrease. In addition, the absence of isoprene could also reduce RO_2 concentration by ~20%, suggesting that isoprene was an important source of RO_2 at DSL site. As for HO_2, drastic decrease of ~53% was found in S1. The above-mentioned decrease in RO*x* obviously could not be explained solely by the removal of isoprene-related radicals. Sensitivity assessment of the model results shows that OVOC concentrations decreased drastically (~41%) after cutting isoprene (e.g. ~37% decrease in formaldehyde, ~65% decrease in methylglyoxal, ~51% decrease in glyoxal, ~100% decrease in methacrolein (MACR), and ~100% decrease in methyl vinyl ketone (MVK)). The decrease in OVOC can further pull-down substantial amount of primary RO_2 and HO_2 (Figure 6 and Figure 9). It is interesting to note that, taking away isoprene also causes a drop of NO_3 (~23%). This result can be attributed to the decrease of secondary production of O_3 (~35%), which can further reduce the formation of NO_3 especially at night.

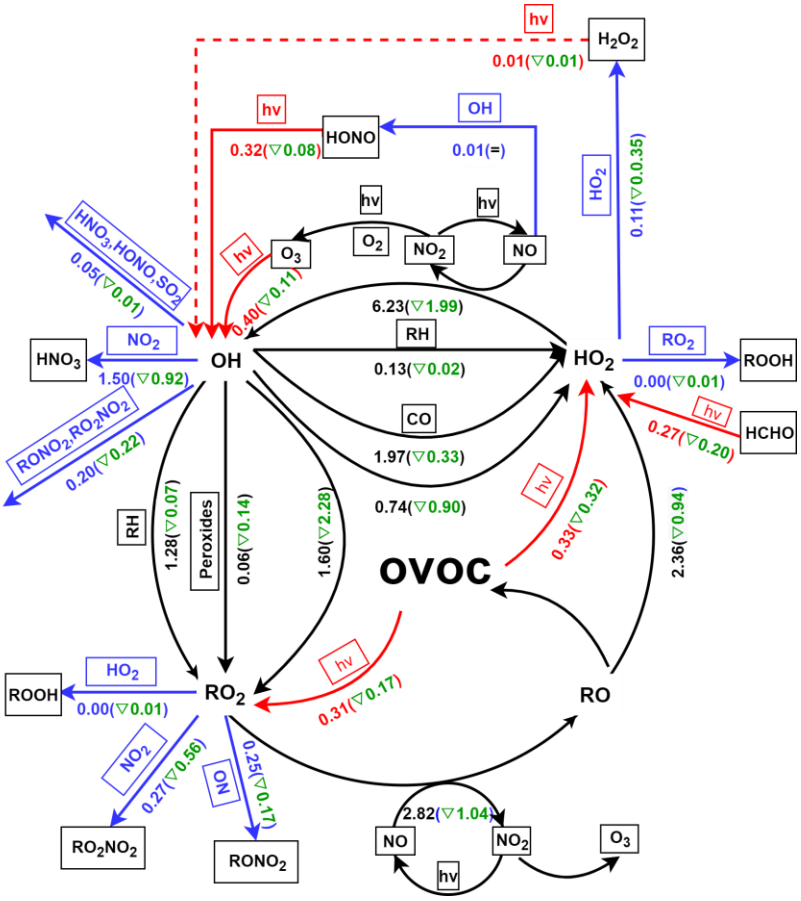

Figure 9. Summary of daytime (06:00-18:00) average budgets of RO*x* radicals (in ppbv h^{-1}) in S1. Primary RO*x* sources and sinks are in red and blue, respectively, and the black lines represent the processes in RO*x* and NO*x* recycling. Values in the brackets represent the difference between S1 and S0.

3.6.2 Impact on O_3 formation

To investigate the detailed impact of isoprene on O_3 formation, the production and sink pathways of O_3 in S1 was also quantified (see Figure 7 (B)). Notably, the simulated maximum and daily average O_3 dropped to 84.95 and 41.23 ppbv, respectively, which is ~35% and ~34% lower than that in S0. By comparing S1 and S0, the absence of isoprene can reduce all the production and sink pathways of O_3. For example, the rate of the two major production pathways of O_3 (HO_2+NO and RO_2+NO) decreased by ~37% and ~45%, respectively. This can be attributed to the drop in the concentration of HO_2 and RO_2 racial in S1. Similarly, the absence of isoprene in O_3 depletion caused a decrease of 0.31 ppbv h^{-1} in the reaction rate of alkene+O_3/NO_3, followed by RO_2+NO_2 (0.22 ppbv h^{-1}) and NO_2+OH (0.265 ppbv h^{-1}). Apparently, the absence of isoprene will reduce the total concentrations of alkenes and can further lead to the decrease of RO_2 and OH level, which ultimately slows down the depletion pathways of O_3. Eventually, the absence of isoprene caused a decrease of 5.78 ppbv h^{-1} in the daytime mean net production rate of O_3. Hence, isoprene chemistry plays an important role in the local O_3 formation at DSL site.

3.6.3 Impact on HCHO formation

The analysis of S0 revealed the important role of isoprene, aromatics, and alkenes in the production of HCHO. To investigate the chain effect of isoprene chemistry on HCHO production, the major reactions that dominate the formation and depletion of HCHO in S1 were also analyzed by OBM model (Figure 8 (B)). Comparisons between S0 and S1 shows that the daily average HCHO decreased by 2.90 ppbv (~39%) when isoprene chemistry is cut off. Obviously, the drop in HCHO concentration cannot be solely illustrated by the absence of RO (from isoprene). As aforementioned, the absence of isoprene slows down the recycling of RO*x*

and can further lead to decrease in RO*x* concentration. Based on the OBM analysis, the concentration of CH_3O, RO (from aromatics), RO (from alkanes), and RO (from alkenes) decreased by 2.70×10^{2} molecule cm^{-3}, 1.59×10^{5} molecule cm^{-3}, 3.35×10^{1} molecule cm^{-3}, and 3.44 molecule cm^{-3}, respectively. The drop in the HCHO precursor concentrations ultimately led to decrease in the daytime reaction rate of $CH_3O + O_2$, RO (from alkenes) + O_2, and RO (from aromatics) + O_2 by 0.66 ppbv h^{-1} (~36%), 0.06 ppbv h^{-1} (~16%), and 0.06 ppbv h^{-1} (~40%), respectively. The total daytime formation rate of HCHO dropped to 1.71 ppbv h^{-1} from 1.66 ppbv h^{-1} (~49%) lower than that in S0. As a result of the lower HCHO and OH concentration in S1, the daily mean depletion rate of HCHO decreased by 1.25 ppbv h^{-1} (~49%). Ultimately, the absence of isoprene pulled down the daily average HCHO level by 1.61ppbv (~36%).

3.7 Uncertainty analysis

Due to limitations in the observations, several issues should be noted in the application of the OBM model to evaluate the local chemistry in the present study. Firstly, methane concentration, which was set to 1850 ppbv based on previous observations, could be an overestimation or underestimation. Thus, we conducted sensitivity analysis of modelled O_3, OH, and HCHO with different methane values (from 1600 ppbv to 1900 ppbv) (Figure. S7). The model predicted O_3, HCHO, and OH concentration with negligible change under different CH_4 values. Secondly, the photolysis rates directly influence the key photochemical processes during the day. Since the photolysis rates were not measured during the sampling period, we also conducted sensitivity analysis by increasing or decreasing the photolysis rates by 20% and 40%. Results showed that the O_3, HCHO and OH concentration could increase by 51.14%, 34.52%, and 50.38%, respectively, when photolysis rates were increased by 40% (Figure S8). On the contrary, when photolysis rates were decreased by 40%, O_3, HCHO and OH concentration decreased by 50.59%, 30.84%, and 47.24%, respectively (Figure. S6). According

to the study by Xu et al. (2013), NO_2 concentration measured by the molybdenum oxide converter technique can be significantly overestimated in areas far away from fresh NO*x* emission sources. Therefore, OBM simulations with reduced NO_2 concentrations were conducted. The results suggest that decreasing NO_2 could increase or decrease of O_3, HCHO and OH concentrations under different scenarios (Figure S9). Overall, decreasing NO_2 by 40% could cause 6.94%, 12.07%, and 6.29% increase in O_3, HCHO, and OH concentrations, respectively. Finally, the total surface area of aerosols was obtained from the study of Wang et al. (2014) and the uncertainty of this value could directly influence the heterogeneous reactions in this model. Therefore, we conducted sensitive analysis by using increasing or decreasing SA value by 40% (Figure S10). The results show that O_3, HCHO, and OH concentrations did not exhibit obvious changes when SA changed. Hence, accurate measurement data of photolysis rate and NO_2 concentration is strongly recommended in further OBM analyses.

4. Conclusions

Our observations at a suburban site of the YRD region from April to June in 2018 captured 5 typical local O_3 formation episodes. The detailed atmospheric photochemistry during these episodes were analyzed by a typical 0-D box model on a local scale. Under stagnant conditions, the photolysis of OVOC served as the predominant primary RO*x* sources. RO*x* achieves efficient recycling with the participation of NO*x*. Influenced by the fast RO*x* recycling, local O_3 was efficiently produced and accumulated under stagnant conditions. The reactions of RO radicals with O_2 dominate the photochemical formation of HCHO. The higher atmospheric oxidative capacity lead to fast degradation of VOCs, which can further lead to high levels of HCHO at the DSL site. Specifically, the degradation of RO radicals (e.g. ISOP34O, ISOPDO, ISOPAO and ISOPBO) from isoprene oxidation play an important role in the photochemical production of HCHO. To investigate the role of isoprene in RO*x* recycle and the formation of secondary pollutant, a sensitivity scenario without isoprene (S1) input was simulated by OBM

model. By comparing S1 to the standard simulation (S0), we find that isoprene chemistry is important in local RO*x* recycling. The absence of isoprene can obviously decrease the concentrations of OVOC and the reaction rates in RO*x* propagations, and further reduce the concentrations of radicals (e.g. OH, HO_2, RO_2). Our results indicate that isoprene chemistry can strongly influence the formation of O_3 and HCHO in the presence of NO*x*. Therefore, removing isoprene can slow down the reaction of HO_2+NO and RO_2+NO by ~37% and ~45%, respectively, and eventually cause ~34% decrease of O_3. As a result of the lower O_3 concentration, average concentration of NO_3 dropped by 23% in S1. The absence of isoprene can also lead to the decrease of RO (from isoprene) and RO*x* concentration and cause an obvious drop of HCHO formation (~49%). Furthermore, other biogenic VOCs (BVOCs, such as terpene and sesquiterpene) can also affect local chemistry via photochemical processes, but those BVOCs were not able to be synchronously observed. Therefore, future studies should take into account those BVOCs. Additionally, the uncertainty analysis conducted in this study indicates the significance of synchronous and accurate observation of photolysis rates and NO_2 concentration when using the OBM. Generally, this study underlines the significant role of isoprene chemistry in radical chemistry, photochemical reactions, and secondary pollutant formation in the atmosphere of the YRD region and provides insights into secondary pollution and its formation mechanisms.

Data availability. The data that support the results are available from the corresponding author upon request.

Authorship contribution. Kun Zhang: Formal analysis, Methodology, Writing-original draft. Ling Huang: Writing-review. Qing Li: Formal analysis. Juntao Huo: Formal analysis, Data curation. Yusen Duan: Formal analysis, Data curation. Yuhang Wang: Writing-review. Elly Yaluk: Formal analysis. Yangjun Wang: Formal analysis. Qingyan Fu: Formal analysis. Li Li: Conceptualization, Methodology, Writing-review & editing.

Competing interest. The authors declare that they have no known competing financial interests or personal relationships that could have appeared to influence the word reported in this paper.

Acknowledgements. This study is supported by the National Natural Science Foundation of China (No. 42075144; No.41875161), Shanghai International Science and Technology Cooperation Fund (No. 19230742500), Shanghai Science and Technology Fund (No. 19DZ1205007), Shanghai Sail Program (NO.19YF1415600), and the National Key Research and Development Program of China (NO.2018YFC0213600). Y. Wang was supported by the National Science Foundation. We thank Shanghai Environmental Monitoring Center (SEMC) for conducting the measurement and sharing the data.

Financial support. This study was financially supported by the National Natural Science Foundation of China (NO. 41875161; NO.42075144), Shanghai International Science and Technology Cooperation Fund (NO. 19230742500), Shanghai Science and Technology Fund (No. 19DZ1205007), Shanghai Sail Program (NO.19YF1415600), and the National Key Research and Development Program of China (NO.2018YFC0213600). Y. Wang was supported by the National Science Foundation.

References

Atkinson, R., and Arey, J.: Atmospheric degradation of volatile organic compounds, Chemical reviews, 103, 4605-4638, 2003.

Atkinson, R., Baulch, D. L., Cox, R. A., Crowley, J. N., Hampson, R. F., Hynes, R. G., Jenkin, M. E., Rossi, M. J., and Troe, J.: Evaluated kinetic and photochemical data for atmospheric chemistry: Volume II - Gas phase reactions of organic species, Atmospheric Chemistry and Physics, 6, 3625-4055, 10.5194/acp-6-3625-2006, 2006.

Chan, K. L., Wang, S. S., Liu, C., Zhou, B., Wenig, M. O., and Saiz-Lopez, A.: On the summertime air quality and related photochemical processes in the megacity Shanghai, China, Science of the Total Environment, 580, 974-983, 2017.

D'Ambro, E. L., Møller, K. H., Lopez-Hilfiker, F. D., Schobesberger, S., Liu, J., Shilling, J. E., Lee, B. H., Kjaergaard, H. G., and Thornton, J. A.: Isomerization of second-generation isoprene peroxy radicals: Epoxide formation and implications for secondary organic aerosol yields, Environmental science & technology, 51, 4978-4987, 2017.

Gong, D., Wang, H., Zhang, S., Wang, Y., Liu, S. C., Guo, H., Shao, M., He, C., Chen, D., He, L., Zhou, L., Morawska, L., Zhang, Y., and Wang, B.: Low-level summertime isoprene observed at a forested mountaintop site in southern China: implications for strong regional atmospheric oxidative capacity, Atmospheric Chemistry and Physics, 18, 14417-14432, 10.5194/acp-18-14417-2018, 2018.

He, Z. R., Wang, X. M., Ling, Z. H., Zhao, J., Guo, H., Shao, M., and Wang, Z.: Contributions of different anthropogenic volatile organic compound sources to ozone formation at a receptor site in the Pearl River Delta region and its policy implications, Atmospheric Chemistry and Physics, 19, 8801-8816, 2019.

585 Jenkin, M. E., Young, J. C., and Rickard, A. R.: The MCM v3.3.1 degradation scheme for
586 isoprene, Atmospheric Chemistry and Physics, 15, 11433-11459, 10.5194/acp-15-11433-
587 2015, 2015.
588 Li, X., Rohrer, F., Brauers, T., Hofzumahaus, A., Lu, K., Shao, M., Zhang, Y. H., and Wahner,
589 A.: Modeling of HCHO and CHOCHO at a semi-rural site in southern China during the
590 PRIDE-PRD2006 campaign, Atmospheric Chemistry and Physics, 14, 12291-12305,
591 10.5194/acp-14-12291-2014, 2014.
592 Li, Y., Shao, M., Lu, S., Chang, C. C., and Dasgupta, P. K.: Variations and sources of ambient
593 formaldehyde for the 2008 Beijing Olympic games, Atmospheric Environment, 44, 2632-
594 2639, 10.1016/j.atmosenv.2010.03.045, 2010.
595 Li, L., An, J. Y., Yan, R. S., Huang, C., Wang, H. L., Lou, S. R., Huang, L., Yarwood, G.
596 Ozone source apportionment over the Yangtze River Delta region, China: Investigation of
597 regional transport, sectoral contributions and seasonal differences. Atmospheric
598 Environment, 202, 269-280, 2019.
599 Li, L., An, J. Y., Shi, Y. Y., Zhou, M., Yan, R. S., Huang, C., Wang, H. L., Lou, S. R., Wang,
600 Q., Lu, Q., Wu, J. Source apportionment of surface ozone in the Yangtze River Delta, China
601 in the summer of 2013. Atmospheric Environment, 144, 194-207, 2016.
602 Lin, H., Wang, M., Duan, Y., Fu, Q., Ji, W., Cui, H., Jin, D., Lin, Y., and Hu, K.: O_3 sensitivity
603 and contributions of different nmhc sources in O_3 formation at urban and suburban sites in
604 Shanghai, Atmosphere, 11, 1-18, 10.3390/atmos11030295, 2020.
605 Liu, X., Lyu, X., Wang, Y., Jiang, F., and Guo, H.: Intercomparison of O_3 formation and radical
606 chemistry in the past decade at a suburban site in Hong Kong, Atmospheric Chemistry and
607 Physics, 19, 5127-5145, 10.5194/acp-19-5127-2019, 2019.

Liu, Y. J., Herdlinger-Blatt, I., McKinney, K. A., and Martin, S. T.: Production of methyl vinyl ketone and methacrolein via the hydroperoxyl pathway of isoprene oxidation, Atmospheric Chemistry and Physics, 13, 5715-5730, 10.5194/acp-13-5715-2013, 2013.

Liu, Z., Wang, Y., Gu, D., Zhao, C., Huey, L. G., Stickel, R., Liao, J., Shao, M., Zhu, T., Zeng, L., Amoroso, A., Costabile, F., Chang, C. C., and Liu, S. C.: Summertime photochemistry during CAREBeijing-2007: RO*x* budgets and O_3 formation, Atmospheric Chemistry and Physics, 12, 7737-7752, 2012.

Riedel, T. P., Wolfe, G. M., Danas, K. T., Gilman, J. B., Kuster, W. C., Bon, D. M., Vlasenko, A., Li, S.-M., Williams, E. J., Lerner, B. M., Veres, P. R., Roberts, J. M., Holloway, J. S., Lefer, B., Brown, S. S., and Thornton, J. A. (2014). An MCM modeling study of nitryl chloride ($ClNO_2$) impacts on oxidation, ozone production and nitrogen oxide partitioning in polluted continental outflow, Atmos. Chem. Phys., 14, 3789–3800, https://doi.org/10.5194/acp-14-3789-2014.

Tan, Z. F., Lu, K. D., Jiang, M. Q., Su, R., Wang, H. L., Lou, S. R., Fu, Q. Y., Zhai, C. Z., Tan, Q. W., Yue, D. L., Chen, D. H., Wang, Z. S., Xie, S. D., Zeng, L. M., and Zhang, Y. H.: Daytime atmospheric oxidation capacity in four Chinese megacities during the photochemically polluted season: a case study based on box model simulation, Atmospheric Chemistry and Physics, 19, 3493-3513, 2019.

Wennberg, P. O., Bates, K. H., Crounse, J. D., Dodson, L. G., McVay, R. C., Mertens, L. A., Nguyen, T. B., Praske, E., Schwantes, R. H., Smarte, M. D., St Clair, J. M., Teng, A. P., Zhang, X., and Seinfeld, J. H.: Gas-phase reactions of isoprene and its major oxidation products, Chemical Reviews, 118, 3337-3390, 2018.

Wolfe, G. M., Kaiser, J., Hanisco, T. F., Keutsch, F. N., de Gouw, J. A., Gilman, J. B., Graus, M., Hatch, C. D., Holloway, J., Horowitz, L. W., Lee, B. H., Lerner, B. M., Lopez-Hilifiker, F., Mao, J., Marvin, M. R., Peischl, J., Pollack, I. B., Roberts, J. M., Ryerson, T. B.,

633 Thornton, J. A., Veres, P. R., and Warneke, C.: Formaldehyde production from isoprene
634 oxidation across NO*x* regimes, Atmospheric Chemistry and Physics, 16, 2597-2610,
635 10.5194/acp-16-2597-2016, 2016a.
636 Wolfe, G. M., Marvin, M. R., Roberts, S. J., Travis, K. R., and Liao, J.: The Framework for 0-
637 D Atmospheric Modeling (F0AM) v3.1, Geoscientific Model Development, 9, 3309-3319,
638 10.5194/gmd-9-3309-2016, 2016b.
639 Xu, Z., Wang, T., Xue, L. K., Louie, P. K. K., Luk, C. W. Y., Gao, J., Wang, S. L., Chai, F. H.,
640 and Wang, W. X.: Evaluating the uncertainties of thermal catalytic conversion in measuring
641 atmospheric nitrogen dioxide at four differently polluted sites in China, Atmos. Environ.,
642 76, 221–226, 2013.
643 Xue, L., Wang, T., Gao, J., Ding, A., Zhou, X., Blake, D. R., Fang, X., Saunders, S. M., Fan,
644 S., Zuo, H., Zhang, Q., Wang, W. Ground-level ozone in four Chinese cities: precursors,
645 regional transport and heterogeneous processes. Atmospheric chemistry and physics, 14(23),
646 13175-13188, 2014.
647 Xue, L., Gu, R., Wang, T., Wang, X., Saunders, S., Blake, D., Louie, P. K. K., Luk, C. W. Y.,
648 Simpson, I., Xu, Z., Wang, Z., Gao, Y., Lee, S., Mellouki, A., and Wang, W.: Oxidative
649 capacity and radical chemistry in the polluted atmosphere of Hong Kong and Pearl River
650 Delta region: Analysis of a severe photochemical smog episode, Atmospheric Chemistry
651 and Physics, 16, 9891-9903, 10.5194/acp-16-9891-2016, 2016.
652 Yang, X., Xue, L. K., Wang, T., Wang, X. F., Gao, J., Lee, S. C., Blake, D. R., Chai, F. H., and
653 Wang, W. X.: Observations and explicit modeling of summertime carbonyl formation in
654 Beijing: identification of key precursor species and their impact on atmospheric oxidation
655 chemistry, Journal of Geophysic Research:Atmosphere, 123, 1426-1440, 2018.

Yang, X., Zhang, G. Q., Sun, Y. M., Zhu, L., Wei, X. F., Li, Z., and Zhong, X. L.: Explicit modeling of background HCHO formation in southern China, Atmospheric Research, 240, UNSP 10494110.1016/j.atmosres.2020.104941, 2020.

Zeng, P., Lyu, X. P., Guo, H., Cheng, H. R., Wang, Z. W., Liu, X. F., and Zhang, W. H.: Spatial variation of sources and photochemistry, of formaldehyde in Wuhan, Central China, Atmospheric Environment, 214, 2019.

Zhang, K., Zhou, L., Fu, Q., Yan, L., Bian, Q., Wang, D., and Xiu, G.: Vertical distribution of ozone over Shanghai during late spring: A balloon-borne observation, Atmospheric environment, 208, 48-60, 2019.

Zhang, K., Li, L., Huang, L., Wang, Y., Huo, J., Duan, Y., Wang, Y., and Fu, Q.: The impact of volatile organic compounds on ozone formation in the suburban area of Shanghai, Atmospheric Environment, 232, 10.1016/j.atmosenv.2020.117511, 2020a.

Zhang, K., Xu, J., Huang, Q., Zhou, L., Fu, Q., Duan, Y., and Xiu, G.: Precursors and potential sources of ground-level ozone in suburban Shanghai, Frontiers of Environmental Science and Engineering, 14, 10.1007/s11783-020-1271-8, 2020b.

Zhu, J., Cheng, H., Peng, J., Zeng, P., Wang, Z., Lyu, X., and Guo, H.: O_3 photochemistry on O_3 episode days and non-O_3 episode days in Wuhan, Central China, Atmospheric Environment, 223, 10.1016/j.atmosenv.2019.117236, 2020a.

Zhu, J., Wang, S. S., Wang, H. L., Jing, S. G., Lou, S. R., Saiz-Lopez, A., and Zhou, B.: Observationally constrained modeling of atmospheric oxidation capacity and photochemical reactivity in Shanghai, China, Atmospheric Chemistry and Physics, 20, 1217-1232, 2020b.

Zong, R. H., Yang, X., Wen, L., Xu, C. H., Zhu, Y. H., Chen, T. S., Yao, L., Wang, L. W., Zhang, J. M., Yang, L. X., Wang, X. F., Shao, M., Zhu, T., Xue, L. K., and Wang, W. X.: Strong ozone production at a rural site in the North China Plain: Mixed effects of urban

681 plumes and biogenic emissions, Journal of Environmental Sciences, 71, 261-270,
682 10.1016/j.jes.2018.05.003, 2018.

683